Cu–TiO$_2$ systems for the photocatalytic H$_2$ production: Influence of structural and surface support features

Sergio Obregón [a], Mario J. Muñoz-Batista [b], Marcos Fernández-García [b], Anna Kubacka [b,*], Gerardo Colón [a,**]

[a] *Instituto de Ciencia de Materiales de Sevilla, Centro Mixto Universidad de Sevilla-CSIC, C/Américo Vespucio s/n, 41092 Sevilla, Spain*
[b] *Instituto de Catálisis y Petroleoquímica, CSIC, C/Marie Curie, 2, Cantoblanco, 28049 Madrid, Spain*

ARTICLE INFO

ABSTRACT

The influence of different TiO$_2$ supports on the Cu active species has been studied. It was found that the photocatalytic H$_2$ evolution is highly affected by the structural and electronic features of surface Cu species. Thus, metal dispersion and oxidation state appears strongly conditioned by the structural and surface properties of the TiO$_2$ support. We have examined three TiO$_2$ supports prepared by different synthetic methods; sol–gel, hydrothermal and microemulsion. In addition, we have induced structural and surface modifications by sulfate pretreatment over freshly prepared TiO$_2$ precursors and subsequent calcination. Notably different copper dispersion and oxidation state is obtained by using these different TiO$_2$ supports. From the wide structural and surface analysis of the catalysts we are able to propose that the occurrence of highly disperse Cu^{2+} species, the sample surface area as well as the crystallinity of the TiO$_2$ support are directly related to the photocatalytic activity for H$_2$ production reaction.

© 2015 Elsevier B.V. All rights reserved.

1. Introduction

The improvement and optimisation of photocatalytic materials is an important task in order to achieve a real application of heterogeneous photocatalysis in the near-future. This handicap is especially crucial if we consider recent energy related applications such as H$_2$ production by photoreforming or CO$_2$ reduction towards valuable fuels [1–5]. The photocatalytic water splitting reaction to produce H$_2$ and O$_2$ using semiconducting catalysts has received much attention due to the potential of this technology, as well as the great economic and environmental interest for the production of the clean fuel H$_2$ from water using solar energy. However, when TiO$_2$ is exploited in hydrogen production using photoreforming reaction, some important difficulties arises. Thus, the rapid recombination process of the photogenerated charge pairs and the occurrence of the eventually backward reactions are considered critical points that still makes this process far from a practical application. Traditionally, highly active photocatalysts are based on TiO$_2$ doped with noble metal ions (Pt, Au, Pd) acting as co-catalysts for charge trapping sites and avoid the electron–hole recombination processes [6–10]. Due to the high cost of such co-catalysts, transi-

tion metal doping with Cu, Fe, Co or Ni have recently turned as a promising option [11–18].

In spite of that obtained rates for these alternative transition metal based systems are still far from those obtained for noble metals, copper based catalysts appear as a promising candidate [16–20]. It can be stated that the origin of the photoactivity for the H$_2$ production reaction of copper-based systems is strongly affected by the complex structural, morphological, and chemical features of copper species [21]. In a recent paper, we concluded the occurrence of highly disperse Cu^{2+} species is directly related to the higher performance of the system for the H$_2$ production reaction [22].

Now we try to present an exhaustive structural and surface characterization of Cu-doped systems using TiO$_2$ supports obtained from different methods; sol–gel, hydrothermal and microemulsion. The intrinsic surface and structural features of the TiO$_2$ support appear to be crucial and strongly affect the final features of copper deposits conditioning in great extent the photoactivity of the system.

2. Experimental

2.1. Catalysts preparation and characterisation

2.1.1. Synthesis by a sol–gel method

TiO$_2$ system was prepared by a sol–gel method using titanium tetraisopropoxide (TTIP) as precursor (10 mL TTIP) in

---

water/isopropanol solution (200 mL iPrOH and 2 mL H_2O). Forced hydrolysis of the TTIP solution was achieved by adding certain volume of bidistilled water (8.4 mL). Finally the pH was adjusted to 9 by adding NH_4OH.

2.1.2. Synthesis by a hydrothermal method

The hydrothermal method followed for TiO_2 preparation can be found elsewhere [23]. Briefly, a TiO_2 colloidal solution was obtained by adding certain amount of Ti^{4+}-isopropanol solution to 400 mL of distilled water at pH 2 achieved by means of acetic acid. After TTiP addition a white precipitate is obtained that upon stirring at room temperature for one week evolves to a milky homogeneous solution. A certain amount of triethylamine (TEA) was then added dropwise to the Ti-solution aliquot till the pH value was 9. Afterwards, the obtained white precipitate suspension was then placed in a Teflon recipient inside of stainless steel autoclave reactor. The hydrothermal treatment was performed at 120 °C, 20 h. The as obtained precipitate was then filtered, repeatedly washed and dried overnight at 120 °C.

2.1.3. Synthesis by a microemulsion method

The titania precursor were obtained by means of a water in oil microemulsion preparation method utilising *n*-heptane (Scharlau) as organic media, Triton X-100 (Aldrich) as surfactant and hexanol (Aldrich) as cosurfactant. Titanium tetraisopropoxide solution with isopropanol (2:3) was added dropwise on the as-prepared microemulsion. Water/Ti and water/surfactant molar ratios were, respectively, 110 and 18 for all samples [24,25]. The resulting mixture was stirred for 24 h, centrifuged, and the separated solid precursors rinsed with methanol and dried at 110 °C for 12 h.

Before copper doping, titania samples were subjected to different calcination treatments. On one hand, the first series of supports was obtained by calcination of as prepared precursor at 400 °C for 2 h. On the other, the second series was previously sulfuric acid pretreated and then calcined at 650 °C for 2 h. This acid pretreatment would stabilize anatase structure and surface area against sintering [26]. Different as prepared TiO_2 samples were denoted as SG, HT and ME referring the preparation method employed (sol–gel, hydrothermal and microemulsion). Moreover the sample labels also indicate the calcination treatment submitted. Thus, i.e. ME650 notation would correspond to TiO_2 sample obtained by microemulsion method and further calcined at 650 °C (calcination at such temperature would imply sulfuric acid pre-treatment).

Then, copper doping has been performed by means chemical reduction using $Cu(NO_3)_2$ as copper precursor and $NaBH_4$ as reducing agent. Thus, 1 g of TiO_2 or $STiO_2$ (calcined at 400 °C and 650 °C, respectively) was dispersed in 100 mL of water solution containing the corresponding stoichiometric amount of copper precursor. Then an excess of $NaBH_4$ was added and the dispersion was thoroughly stirred for 1 h at room temperature. Finally, this solution has been filtered and washed with distilled water and the obtained powder dried at 110 °C overnight.

2.2. Characterization techniques

BET surface area measurements were carried out by N_2 adsorption at 77 K using a Micromeritics 2000 instrument.

X-ray diffraction (XRD) patterns were obtained using a Siemens D-501 diffractometer with Ni filter and graphite monochromator. The X-ray source was Cu Kα radiation. From the line broadening of corresponding X-ray diffraction peaks, we have calculated the mean crystallite size according to Scherrer equation.

Diffuse reflectance spectra were obtained on a UV–vis scanning spectrophotometer Shimadzu AV2101, equipped with an integrating sphere, using $BaSO_4$ as reference. UV–vis spectra were performed in the diffuse reflectance mode (*R*) and transformed to

a magnitude proportional to the extinction coefficient (*K*) through the Kubelka–Munk function, $F(R_\propto)$. For the sake of comparison, all spectra were arbitrary normalised in intensity to 1. Band gap values were obtained from the plot of the modified Kubelka–Munk function $(F(R_\propto)E)^{1/2})$ versus the energy of the absorbed light *E*. This considers anatase an indirect gap semiconductor.

XPS data were recorded on 4.4 mm^2 pellets, 0.5 mm thick, prepared by slightly pressing the powdered materials which were outgassed in the prechamber of the instrument at 150 °C up to a pressure <2·10^{-8} torr to remove chemisorbed water from their surfaces. Spectra were recorded using a Leybold–Heraeus LHS-10 spectrometer, working with constant pass energy of 50 eV. The spectrometer main chamber, working at a pressure <2·10^{-9} torr, is equipped with an EA-200 MCD hemispherical electron analyser with a dual X-ray source working with Al Kα ($h\nu$ = 1486.6 eV) at 120 W and 30 mA. C 1s signal (284.6 eV) was used as internal energy reference in all the experiments.

Transmission electron microscopy (TEM) electron microscopy was performed in a Philips CM200 microscope. The samples were dispersed in ethanol using an ultrasonicator and dropped on a carbon grid.

Diffuse reflectance infrared Fourier transform spectra (DRIFTS) were taken in a Bruker Vertex 80 FTIR spectrometer using a MCT detector and running under OPUS/IR software. The set-up consists of a praying mantis DRIFTS accessory (Harrick Scientific) and a reaction cell (HVC, Harrick Scientific). The reaction mixture was prepared by injecting 8000 ppm of methanol (≥99%; Aldrich) into a wet (1:10 methanol to water ratio) N_2 flow before entering the DRIFTS cell. Higher quantities of methanol provide a strong gas-phase IR signal which does not allow to obtain any information of the surface species. The DRIFTS spectra were collected in the range of 4000–600 cm^{-1} with a resolution of 2 cm^{-1}, by averaging 10 scans over a total of 1.2 s. In DRIFTS experiments, in-situ light excitation was carried out using 365 nm (20 nm half-width) radiation.

2.3. Photocatalytic runs

Photocatalytic H_2 production tests were performed in a flow-reactor system. The powder photocatalysts were suspended in a methanol–water solution (300 mL, MeOH 10% v/v in water). The reaction media was continuously thermostated at 23 ± 2 °C to prevent any significant evaporation of the sacrificial agent. The catalyst suspension (0.5 g/L) was firstly degassed with an N_2 stream (150 mL/min) for 30 min. After that the N_2 flow was settled at 15 mL/min and stabilised for 15 min. This nitrogen flow was used to displace the hydrogen produced from the photoreactor headspace towards the GC measuring system. Then, the lamp (125 W medium pressure Hg lamp) was switched on and the effluent gases were analysed to quantify H_2 production by gas chromatography (Agilent 490 micro GC) using a thermal conductivity detector.

3. Results and discussions

The structural features of different samples obtained with TiO_2 and $STiO_2$ series have been studied by X-ray diffraction. In Fig. 1, we show the diffraction patterns obtained for both series, calcined at 400 °C and 650 °C (TiO_2 and $STiO_2$). In all cases, anatase phase was practically the unique crystalline structure detected. Only in the case of the sample obtained from microemulsion method and furtherly calcined at 400 °C a small amount (less than 5%) of brookite phase was detected. Regarding to $STiO_2$ series, in spite of the high calcination temperature rutile phase is not present. Only ME shows a small residual amount that would point out the first step of rutilization process (Fig. 1b). This is due to the well-known stabilization
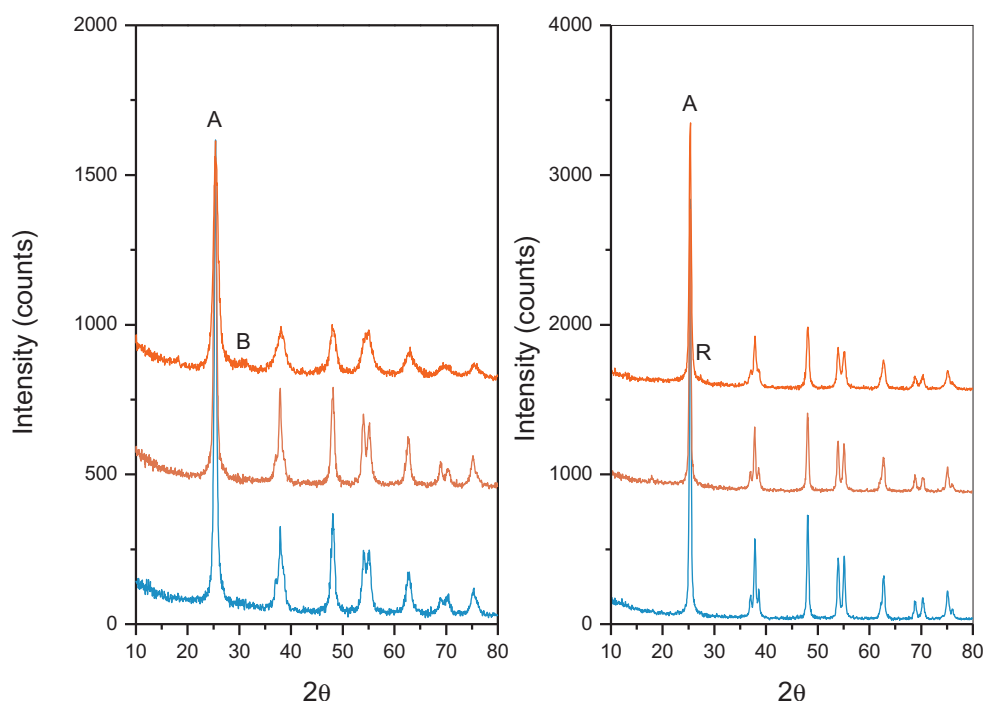
Fig. 1. XRD patterns for (a) CuT400 and (b) CuST650 series of samples.

effect of presulfation treatment on the amorphous precursor [27]. From these patterns the crystallite size has been calculated by using the Scherrer equation. Although in all cases the anatase phase was found as the almost unique crystalline structure, important differences can be noticed in the crystallite sizes of the studied samples (Table 1). Thus, SG and HT samples calcined at 400 °C clearly exhibit crystallite size around 15–20 nm, while ME denotes a notably lower size. So within this series the microemulsion method leads to a lower crystallization degree. This fact is also accompanied by the presence of certain amount of brookite phase which would remain from the anatase formation mechanism. Regarding to STiO$_2$ series calcined at 650 °C it appears that SG and HT samples present again similar crystallite size around 30 nm, while ME denotes a lower crystallization degree.

This structural differentiation is also evidenced by observing the textural properties of all samples (Figs. 2 and 3). As expected calcination at 400 °C preserves in a great extent the surface area values (Table 1). In all cases N$_2$ adsorption-desorption isotherms present a type IV profile indicating the mesoporous character of the samples. The average pore sizes for ME400 lies ca 10 nm, being for SG and HT samples ca 4 nm (Fig. 2b). So the difference in surface values, particularly between SG–HT and ME, is representative of the quite different preparation method employed. In this sense, ME sample

shows a notably high surface area and a relatively higher pore size with respect SG and HT.

Presulfated series presents a notably reduction of the surface area due to the high calcination temperature, being ME the sample exhibiting the lower value. In this case, all samples within the series show similar pore size located at around 15 nm (Fig. 3b). As it can be noticed from surface area values, presulfation process and subsequent calcination at 650 °C seems to markedly affect to ME sample, showing the lowest value of the series denoting the drastic surface collapse of this sample after presulfation and high calcination treatment.

As it can be noticed, although all samples show anatase structure, they exhibit interesting surface and structural feature differences that could condition the Cu deposition by the chemical reduction method. Thus, from TEM study of 650 °C calcined samples interesting evolution of Cu nanoparticle size can be stated (Fig. 4). In fact, one factor that can significantly influence the electronic properties of the nanocomposite is the size of the metal particles. Thus, it was stated that size-dependent shift in the Fermi level of the TiO$_2$–Au nanocomposite influences the photogenerated charge separation [28]. Subramanian et al. stated that the greater change in the Fermi level with smaller Au nanoparticles indicated higher photocatalytic reduction efficiency and photocurrent generation. Thus,

Table 1
Surface and structural properties for different Cu-doped TiO$_2$ systems.

Sample	Calcination temperature (°C)	S_{BET} (m^2/g)	Average pore size (nm)	Pore volume (cm^3/g)	Band-gap (eV)	Crystallite size (nm)[a]	Cu/Ti from EDX
Cu2T–SG	400 °C	74	4	0.1865	3.10	18	0.032
Cu2T–HT		78	9	0.2865	2.99	15	0.045
Cu2T–ME		102	4	0.1265	2.86	8	0.040
Cu2ST–SG	650 °C	33	15	0.1783	3.06	33	0.035
Cu2ST–HT		35	25	0.2027	2.95	30	0.035
Cu2ST–ME		20	15	0.1215	2.87	24	0.040

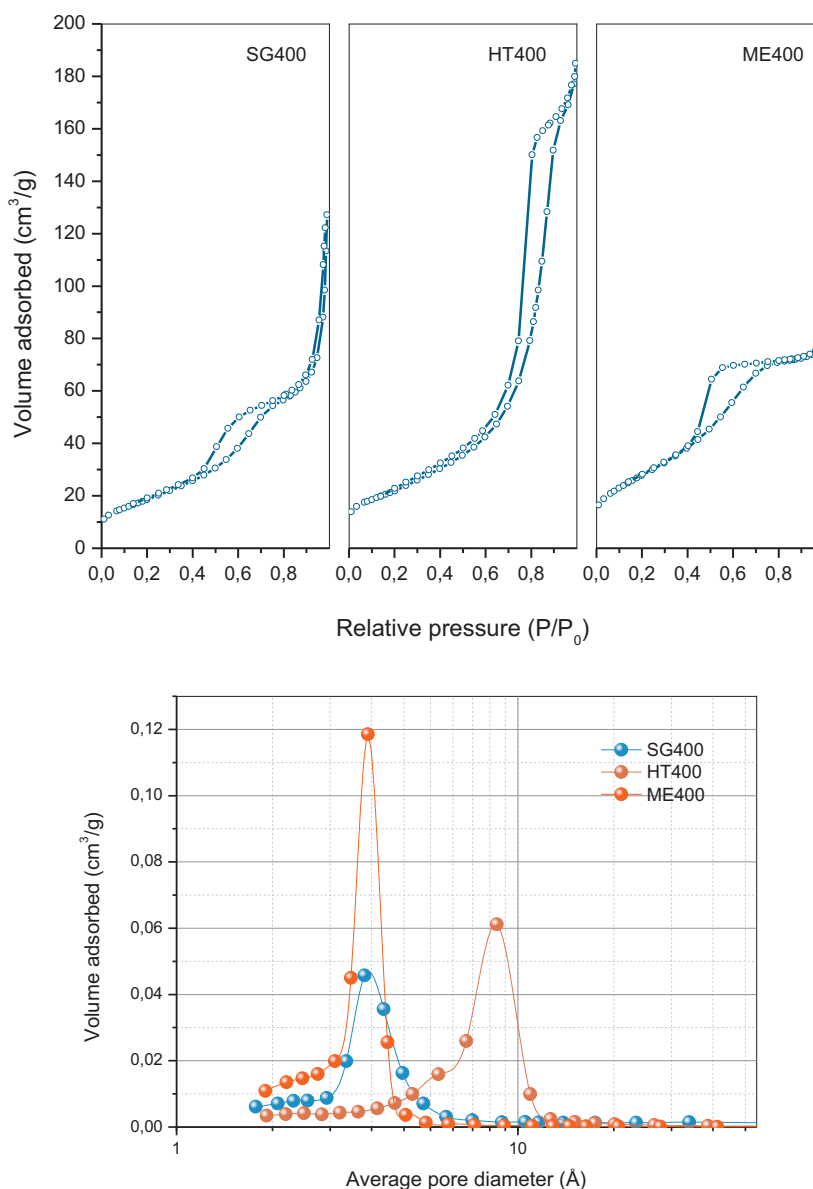[a] Anatase crystallite size measured from XRD peak broadening for (1 0 1) reflexion.

Fig. 2. (a) N_2 adsorption–desorption isotherms and (b) pore size distribution curves for CuT400 series.

size control is of great importance for optimising the photocatalytic activity in nanocomposite photocatalysts.

Samples calcined at 400 °C do not show any evidence of the presence of Cu nanoparticle, probably due to the notably low size of the Cu particles. It is worthy to note that SG650 shows a narrow distribution with the lowest Cu average particle size centered at 1–2 nm. This particle size value is similar to that obtained by Moon et al. by using polyacrylic acid modified TiO_2 [29]. On the contrary, HT650 and ME650 exhibit average Cu particle size 3–4 nm. Thus, it is possible to state that Cu size follows the following order: SG650 < HT650 ≈ ME650.

In Fig. 5, we depict the hydrogen production rates for all the Cu-doped samples studied. As it can be noted the hydrogen production reaches a stable value after the first 45 min. (Fig. 5a). It is clear that although a similar deposition method has been employed and a similar Cu content is present in all samples, the particular features of both support and surface Cu species notably affect to the final photocatalytic performance (Fig. 5c). Moreover, since the different TiO_2 supports showed quite unlike surface area values we also included the specific production rate per surface area (Fig. 5d).

In order to assess the situation of Cu species at the surface and elucidate how it could affect to the photoactivity, we have performed XPS analysis of all samples (Table 2). In all cases, the Cu 2p curve is formed by two peaks located at ca. 932 and 953 eV which can be ascribed to Cu $2p_{3/2}$ and Cu $2p_{1/2}$, respectively (Fig. 6). Moreover, the presence of the shakeup satellite peak at around 940 eV denotes the occurrence of Cu^{2+} species [30]. From the deconvolution of Cu 2p spectra it is possible to draw information about the composition of Cu^{1+} and Cu^{2+} species at the surface as well the chemical composition of the surface (Table 2). It is worthy to mention that although the Cu nominal contents in all samples are similar (see EDX analysis in Table 1), the Cu/Ti ratio obtained from XPS shows an interesting evolution. It is well-known that X-ray photoelectron spectroscopy (XPS or ESCA), because of its high surface sensitivity (probing depth ca. 2 nm), has been considered as one of the best techniques for studying the dispersion of transition metal oxides on various supports. Thus, Cu-samples calcined at 400 °C clearly exhibit lower Cu/Ti ratios (between 0.14 and 0.18) with respect to high temperature calcined samples (showing Cu/Ti ratios above 0.20). As widely reported in the literature, a
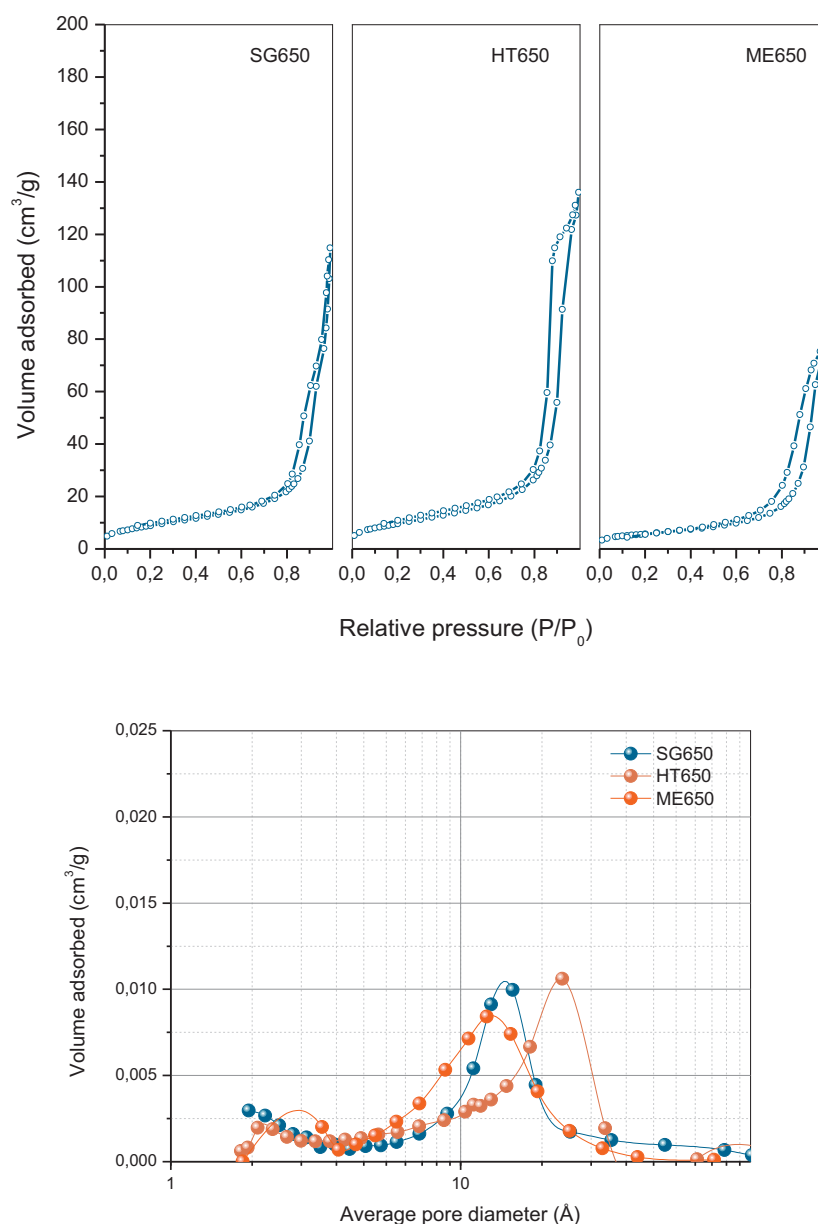
Fig. 3. (a) N_2 adsorption–desorption isotherms and (b) pore size distribution curves for CuST650 series.

lower metal/support ratio could be related to a higher metal dispersion on the support [31–33]. In general, the different dispersion degree is associated to both the surface area of the support and the metal/support interaction [34]. This clearly implies that the dispersion of surface Cu species is quite different depending on the thermal treatment of the support. It can be established that the lower Cu/Ti ratio, the higher dispersion is. Indeed, from TEM

images it was not possible to detect the presence of Cu nanoparticles, denoting the highly disperse situation of Cu species. This fact is quite reasonable by considering the different surface area values of each TiO_2 support (Table 1). In this sense, ME400 sample showed the highest BET surface area value and exhibits the lower Cu/Ti ratio denoting a higher metal dispersion. On the contrary, ME650 sample presents the highest Cu/Ti ratio indicating a high Cu surface

Table 2

XPS analysis for different Cu-doped TiO_2 systems.

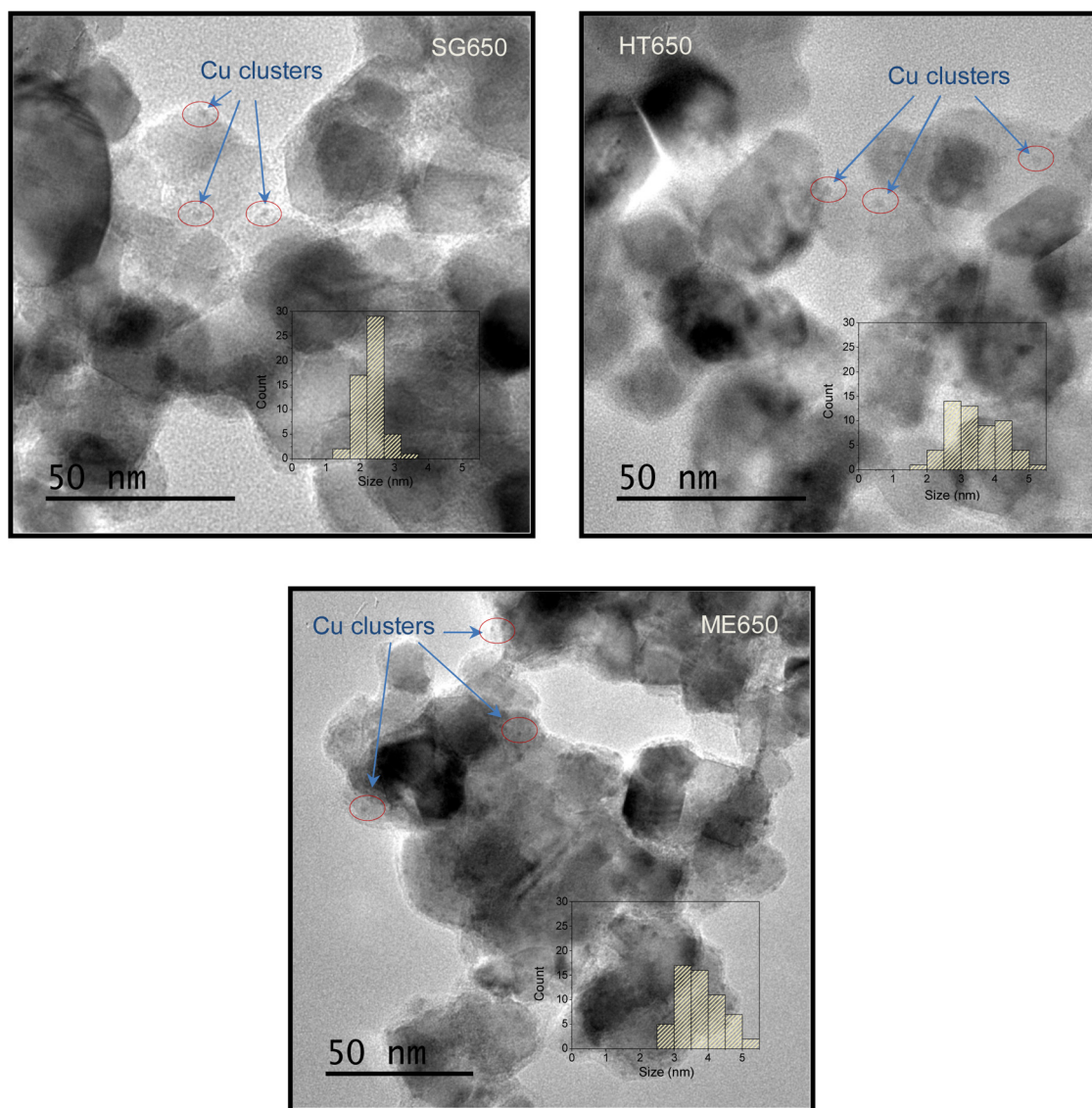| Sample	Calcination temperature (°C)	S_{BET} (m^2/g)	Ti $2p_{3/2}$ (eV)	Cu $2p_{3/2}$ (eV)		I_m/I_s	% Cu^{2+}	Cu/Ti	O/Ti
				Cu^{1+}	Cu^{2+}				
Cu2T–SG	400 °C	74	458.0	932.1	934.1	4.24	41.2	0.183	2.43
Cu2T–HT	400 °C	78	458.4	932.3	934.5	4.20	47.4	0.180	2.44
Cu2T–ME	400 °C	102	458.2	932.2	934.3	3.48	52.0	0.138	2.49
Cu2ST–SG	650 °C	33	458.5	932.3	934.2	3.87	54.0	0.240	2.48
Cu2ST–HT	650 °C	35	458.2	932.0	934.1	3.24	58.0	0.285	2.65
Cu2ST–ME	650 °C	20	458.2	932.2	934.3	3.20	61.5	0.417	2.73

Fig. 4. TEM images for SG650, HT650 and ME650 samples (inset: each TEM image includes the Cu-nanoparticle size distribution).

concentration which can be associated to its lowest surface area. Thus, the first consideration concerns to the surface aggregation of Cu species, which clearly depends on the textural properties of the support.

Moreover, the oxidation state of Cu seems also to be dependent on the surface features. As it can be noticed it appears that the appearance of Cu^{1+} species is somehow related to the Cu dispersion (Fig. 7a). Thus, as the Cu/Ti ratio increases, that is Cu lower dispersion at the surface, the amount of Cu^{1+} trends to diminish. On the contrary, higher Cu species dispersion leads to higher amount of Cu^{1+}. This appears the oxidation state stabilised at the titania–copper interface, as mentioned in previous works [35] and nicely shown in recent dates by Baber et al. [36] On this basis, as the Cu dispersion increases it is possible to stabilize larger quantities of the reduced Cu^{1+} species at the surface. As it has been discussed here and follows from simple considerations, the dispersion of any surface species is in turn correlated with the surface area of the support. Therefore, upon the same doping method the different surface features of the support would drive both the dispersion as well as the oxidation state of Cu species at the surface.

By observing the H_2 production rates obtained the following order can be attained as a function of the support independently of the calcination treatment: SG > HT » ME. Moreover, except for SG650 sample, the calcination at 650 °C leads to lower reaction rates. It is worthy to note that ME400 and ME650 samples showed the lowest values of each series. This could be related in principle to the occurrence of certain crystalline impurities (brookite and rutile, respectively). Although the three crystalline phases of TiO_2 are able to produce hydrogen, anatase appears as the most active phase amongst them [37,38]. In our case the presence of rutile and brookite is residual showing a low crystallization degree. Such low crystallinity impurities would act as recombination center. Indeed, the synergy of mixed phase TiO_2 is strongly dependent of the microstructural situation of the present structures [39–41]. For this reason, although it has been reported that TiO_2 polymorph junctions (anatase–rutile and even anatase–brookite) [42,43] would show improved photocatalytic performance for hydrogen production with respect to single anatase, in our case, it is expected that the residual presence of other phases could be detrimental. In spite of these considerations, other parameters concerning to situation Cu species at the surface might be considered. As previously reported, the occurrence of highly disperse Cu^{2+} species is directly related to
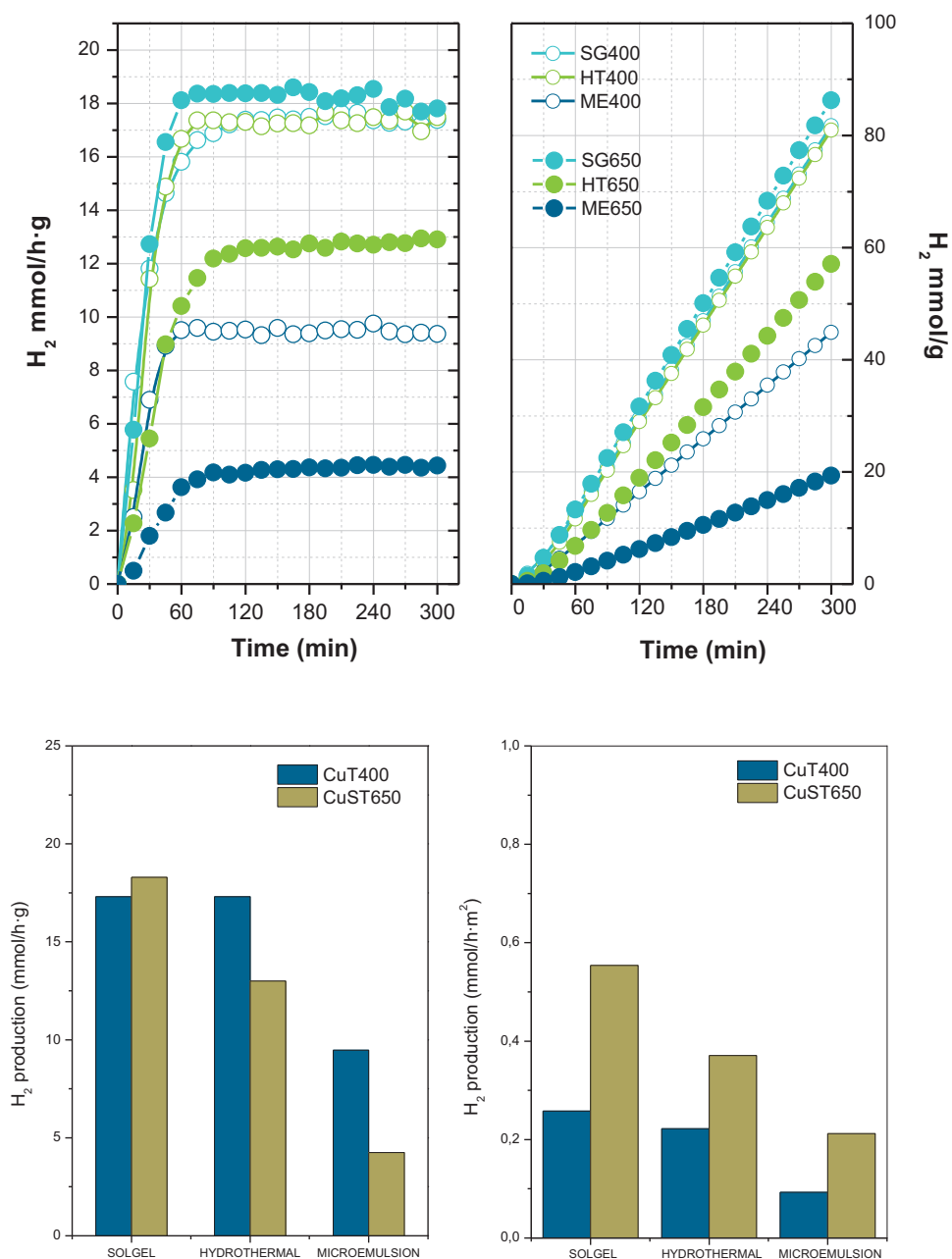
Fig. 5. (a) Evolution of H_2 production rates; (b) H_2 production with time; (c) H_2 production rates for different series; (d) Specific H_2 production rates.
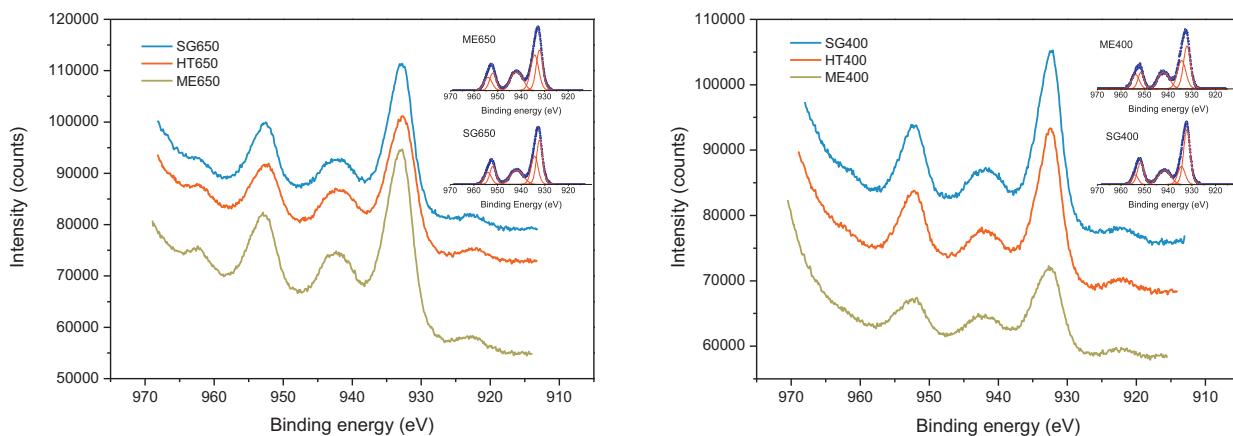

Fig. 6. Cu 2p spectra for (a) T400 and (b) ST650 series (inset: shows the deconvolution of Cu 2p peaks).
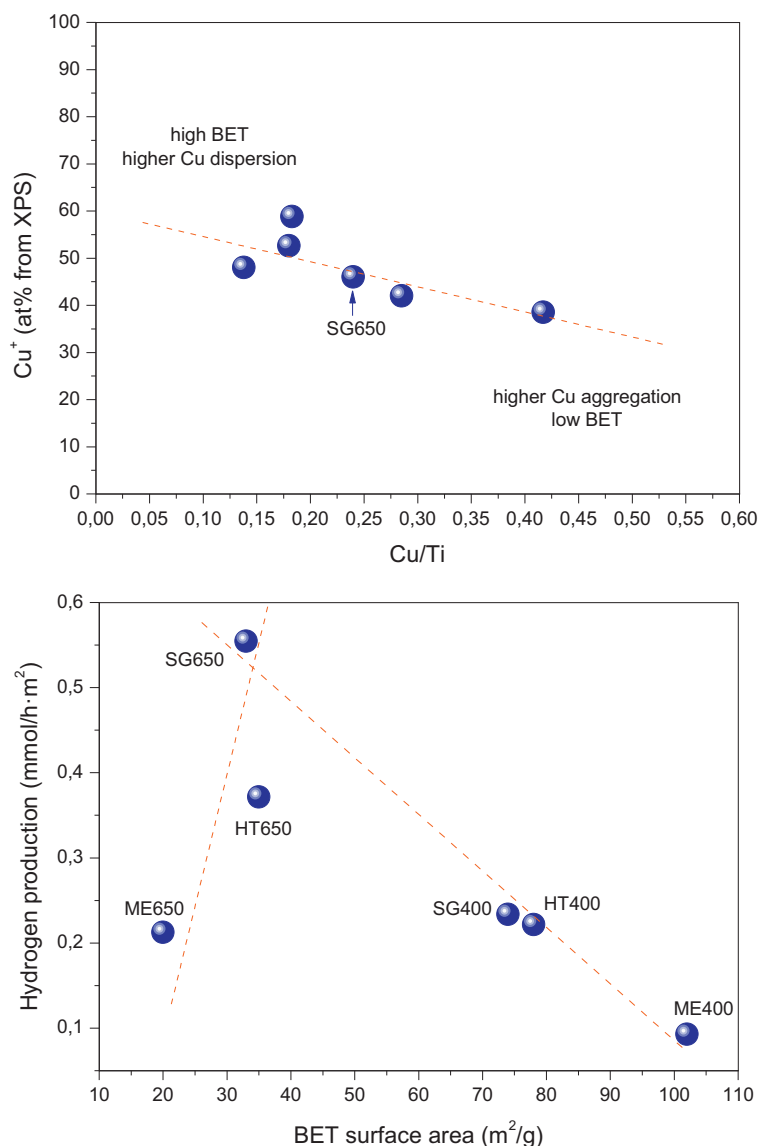
Fig. 7. Evolution of Cu^{1+} surface content with Cu/Ti ratio; (b) Correlation between H$_2$ production rate and BET surface area.

the higher performance of the system for the H$_2$ production reaction. Thus, highly disperse Cu^{2+} species would be easily reduced during the reaction forming Cu^0 sites that will act as an effective co-catalyst for a water reduction reaction [22]. Thus, if we consider the effect of textural support features on the Cu species dispersion and oxidation state (Fig. 7b) it is possible to correlate the optimum photocatalytic performance with a specific value of surface area. At this optimum point (SG650) the sample shows an adequate surface area to provide high dispersion as well as limited average reduction of the copper entities and as the same time a suitable crystallite size, i.e. high crystallinity degree. In this sense, it is clear that the larger CuO$_x$ deposits, contributing to a loss in Cu dispersion with increasing loading, has been correlated with the decreased H$_2$ generation at higher Cu loadings [44,45].

As above mentioned, SG650 sample was the one showing a narrow Cu nanoparticle size distribution centered at ca 1–2 nm. Although HT650 sample also shows similar surface area, the crystallite size is slightly lower and the Cu/Ti ratio appears rather higher than SG650. Moreover, ME650 exhibits the lowest BET surface area and therefore the highest Cu aggregation. In addition, and as it was

mentioned before, this sample also shows a small amount of rutile phase which could hinder at a certain extent the photocatalytic performance. Samples calcined at 400 °C are located at the minimum of the H$_2$ production curve. In spite of the highest surface area values showed by these set of samples, the photocatalytic performance is lower probably due to lower aggregation of Cu species which implies relatively lower presence of Cu^{2+}, as demonstrated here by XPS as well as previous studies of the titania–copper interface [36].

On the basis of this discussion, it is possible to conclude that SG650 sample shows balanced structural, textural features that condition the particular situation of Cu species.

Till this point, we have discussed the effect of Cu species on the surface and how the support features could affect to the photocatalytic performance. In order to assess the effect of the different support itself onto the photoactivity, we have also studied the adsorption and photo-reaction of methanol over selected samples. Fig. 8 shows the result of the in-situ following of the methanol fate under light illumination in presence of water for the two samples showing largest photochemical differences. The figure presents difference spectra (taking as background the previous spectra to $t = 0$ s,
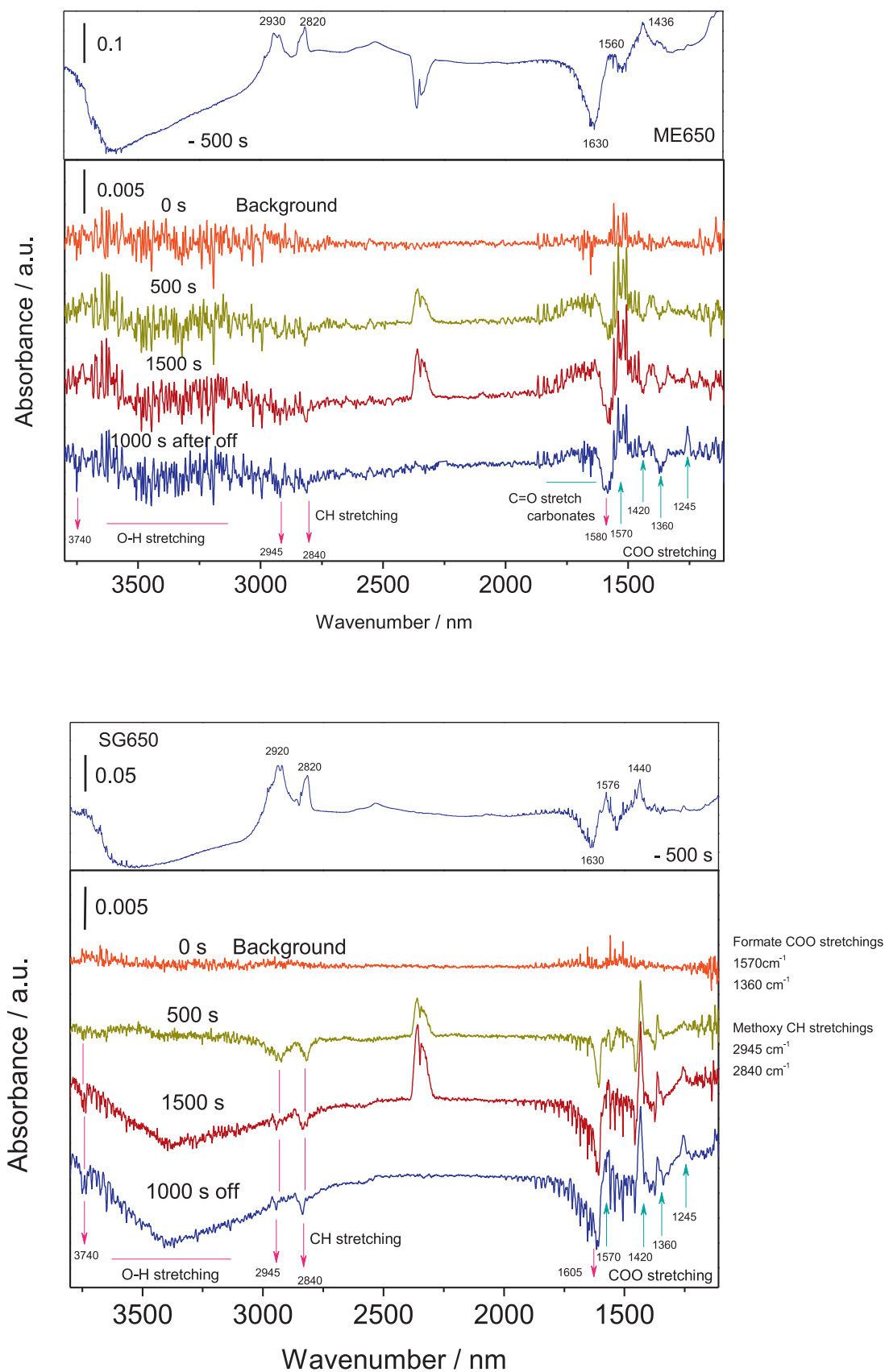
Fig. 8. FTIR spectra for the in-situ analysis of the methanol photo-oxidation on (a) ME650 and (b) SG650 samples.

that is, 1.2 s before) considering; (i) in the upper panel of each plot (sample) the adsorption process of methanol up to surface saturation and (ii) in the lower panel of each plot (sample) the evolution of such species under reaction conditions.

In the upper panels we observed a complex line shape in the C—H stretch region (2980–2800 cm^{-1}) with at least four peaks, although one is not fully resolved and detected only as a shoulder of the main peak of the lower wavenumber region. The C—H region would thus indicate the co-existence of methanol and methoxy species [46]. The dissociate species, presenting the symmetric and asymmetric C—H stretch at the lower wavenumber part of each spectral feature of the region, seems the most important in view of the peaks intensity. These modes are observed with other two at ca. 1575–1560 and 1440–1435 cm^{-1} which likely indicates the presence of carboxylates although the lower wavenumber region must also have contributions for methanol/methoxy species [47].

Under reaction the methanol-related species disappear slowly and this seems to be produced by their chemical evolution. For ME650 the disappearance is rather slow and renders $CO_{2,g}$ (ca. 2250 cm^{-1}) and formate type species with bands at ca. 1570 and 1360 cm^{-1} [48]. At larger reaction times we can see the increasing presence of other carbonates and even other species with carbonyl moieties (formaldehyde, formic acid) as evidenced by the broad bump observed in the 1750–1600 cm^{-1} region [47,49]. Carbonyl moieties are responsible of the intensity for wavenumbers above ca. 1680 cm^{-1}. While it is not possible to ascribe this broad feature to specific species, it is clear the presence of these two types of adsorbates, and thus, the increasing heterogeneity of the surface species with time on stream. Such species indicate, on the other hand, the stay of partially oxidised species at the surface (corroborated by the spectrum obtained at dark conditions) of the materials, without easy progression to the total oxidation product.

In the SG650 case, we show the faster progress of the methanol-type species disappearance and a larger increase in carbon dioxide production. We also observed the presence of formate and some carboxyalates but other species, particularly those indicating partial oxidation organic species containing carbonyl moieties, are strongly diminished with respect to the other sample tested.

So, titania not only plays a role through shaping the copper species dispersion and oxidation state but seems to strongly influence the chemical fate of the photo-hole attack to the sacrificial agent. According to Fig. 8 this could be related to the involvement of hydroxyl species. The evolution of species with O—H stretch at 3740 cm^{-1} or corresponding to associated species (ca. 3400 cm^{-1}) suggest a reordering of the surface which is stable at dark conditions, occurring to a deeper degree in the case of the most active SG650 sample. In any case, what it is clear is the point that the most active system not only handles electrons with the help of copper in a more efficient way but that hole handling is also favoured, probably due to energetic reasons that allow to progress the reaction further, up to the total oxidation product, and does not "poison" the titania surface with organic intermediates.

4. Conclusions

We have prepared a set of Cu-doped TiO_2 by chemical reduction method and using different TiO_2 supports. From the wide structural and surface characterization of the studied samples we can conclude that the occurrence of highly disperse Cu^{2+} species is directly related to the higher performance of the system for H_2 production reaction. Thus, highly disperse Cu^{2+} species would be easily reduced during the reaction forming Cu^0 sites that will act as an effective co-catalyst for water reduction reaction. The intrinsic structural and textural support features strongly affect to the Cu nanoparticle dispersion and subsequently to the Cu oxidation state. Indeed, high

temperature anatase structure, with relatively high surface area would induce an improved charge separation and the handling of both charge carrier species by surface (copper and titania) entities to efficiently produce hydrogen. By a simple surface doping method, we have obtained a notably photocatalytic activity. So, it is clear that the understanding of chemical and structural situation of the whole system, copper and titania, is crucial to design highly active systems.

References

[1] A. Kubacka, M. Fernández-García, G. Colón, Chem. Rev. 112 (2012) 1555–1614.
[2] E.L. Cates, S.L. Chinnapongse, J.H. Kim, Environ. Sci. Technol. 46 (2012) 12316–12328.
[3] J.S. Hwang, J.S. Chang, S.E. Park, K. Ikeue, M. Anpo, Top. Catal. 35 (2005) 311–319.
[4] R. Vinu, G. Madras, Curr. Org. Chem. 17 (2013) 2538–2558.
[5] J.C. Colmenares, R. Luque, Chem. Soc. Rev. 43 (2014) 765–778.
[6] M. Grätzel, R.F. Howe, J. Phys. Chem. 94 (1990) 2566–2572.
[7] X. Li, P.L. Yue, C. Kutal, New J. Chem. 8 (2003) 1264–1269.
[8] A. Naldoni, M. D'Arienzo, M. Altomare, M. Marelli, R. Scotti, F. Morazzoni, E. Selli, V. Dal Santo, App. Catal. B: Environ. 130–131 (2013) 239–248.
[9] A.V. Puga, A. Forneli, H. García, A. Corma, Adv. Funct. Mater. 24 (2014) 241–248.
[10] R. Su, R. Tiruvalam, A.J. Logsdail, Q. He, C.A. Downing, M.T. Jensen, N. Dimitratos, L. Kesavan, P.P. Wells, R. Bechstein, H.H. Jensen, S. Wendt, C.R.A. Catlow, C.J. Kiely, G.J. Hutchings, F. Besenbacher, ACS Nano 8 (2014) 3490–3497.
[11] E. Pulido Melián, M. Nereida Suárez, T. Jardiel, J.M. Doña Rodríguez, A.C. Caballero, J. Araña, D.G. Calatayud, O. González Díaz, Appl. Catal. B: Environ. 152–153 (2014) 192–201.
[12] R. Dholam, N. Patel, M. Adami, A. Miotello, Int. J. Hydrogen Energy 34 (2009) 5337–5346.
[13] K. Lalitha, G. Sudanandam, V.D. Kumari, M. Subrahmanyan, B. Sreedhar, N.Y. Heblakar, J. Phys. Chem. C 114 (2010) 22181–22189.
[14] C. Ampelli, R. Passalacqua, C. Genovese, S. Perathoner, G. Centi, T. Montini, V. Gombac, J.J. Delgado Jaen, P. Fornasiero, RSC Adv. 3 (2013) 21776–21788.
[15] S. Oros-Ruiz, R. Zanella, S.E. Collins, A. Hernández-Gordillo, R. Gómez, Catal. Commun. 47 (2014) 1–6.
[16] Z. Wang, Y. Liu, D.J. Martin, W. Wang, J. Tang, H. Huang, Phys. Chem. Chem. Phys. 15 (2013) 14956–14960.
[17] D.P. Kumar, M.V. Sankar, M.M. Kumari, G. Sadanandam, B. Srinivas, V. Durgakumari, Chem. Commun. 49 (2013) 9443–9447.
[18] L. Clarizia, D. Spasiano, I. Di Somma, R. Marotta, R. Andreozzi, D.D. Dionysiou, Int. J. Hydrogen Energy 39 (2014) 16812–16831.
[19] L.S. Yoong, F.K. Chong, B.F. Dutta, Energy 34 (2009) 1652–1661.
[20] C. Wang, Q. Hu, J. huang, C. Zhu, Y. Cao, Appl. Surf. Sci. 292 (2014) 161–164.
[21] A. Kubacka, M.J. Muñoz-Batista, M. Fernández-García, S. Obregón, G. Colón, Appl. Catal. B: Environ. 163 (2015) 214–222.
[22] J.M. Valero, S. Obregón, G. Colón, ACS Catal. 4 (2014) 3320–3329.
[23] M.C. Hidalgo, M. Aguilar, M. Maicu, J.A. Navío, G. Colón, Catal. Today 129 (2007) 50.
[24] A. Kubacka, G. Colón, M. Fernández-García, Catal. Today 143 (2009) 286–292.
[25] A. Kubacka, A. Bachiller-Baeza, G. Colón, M. Fernández-García, Appl. Catal. B 93 (2010) 274–281.
[26] G. Colón, J.M. Sánchez-España, M.C. Hidalgo, J.A. Navío, J. Photochem. Photobiol. A: Chem. 179 (2006) 20–27.
[27] G. Coloín, M.C. Hidalgo, G. Munuera, I. Ferino, M.G. Cutrufello, J.A. Navío, Appl. Catal. B 63 (2006) 45–59.
[28] V. Subramanian, E.E. Wolf, P.V. Kamat, J. Am. Chem. Soc. 126 (2004) 4943–4950.
[29] G.D. Moon, J.B. Joo, I. Lee, Y. Yin, Nanoscale 6 (2014) 12002–12008.
[30] M. Zhu, M.L. Du, D.L. Yu, Y. Wang, N.L. Wang, M.L. Zou, M. Zhang, Y.Q. Fu, J. Mater. Chem. A 1 (2013) 919–923.
[31] B.M. Reddy, B. Chowdhury, E.P. Reddy, A. Fernández, Appl. Catal. A: Gen. 213 (2001) 279–288.
[32] M. Ilie, B. Cojocaru, V.I. Parvulescu, H. Garcia, Int. J. Hydrogen Energy 36 (2011) 15509–15518.
[33] A.M. Tarditi, N. Barroso, A.E. Galetti, L.A. Arrúa, L. Cornaglia, M.C. Abello, Surf. Interface Anal. 46 (2014) 521–529.

[34] I. Rossetti, C. Biffi, C.L. Bianchi, V. Nichele, M. Signoretto, F. Menegazzo, E. Finocchio, G. Ramis, A. Di Michele, Appl. Catal. B: Environ. 150–151 (2014) 12–20.

[35] A. Kubacka, M. Muñoz-Batista, M. Ferrer, M. Fernández-García, Appl. Catal. B 140–141 (2013) 680–690.

[36] A.E. Baber, X. Yang, H.Y. Kim, K. Mudiyanselage, M. Soldemo, J. Weissenrieder, S.D. Senanayake, A. Al-Mahboob, J.T. Sadowski, J. Evans, J.A. Rodríguez, P. Liu, F.M. Hoffmann, J.G. Chen, D.J. Stacchiola, Angew. Chem. Int. Ed. 53 (2014) 5336–5340.

[37] G.L. Chiarello, A. Di Paola, L. Palmisano, E. Selli, Photochem. Photobiol. Sci. 10 (2011) 355–360.

[38] M. Murdoch, G.I.N. Waterhouse, M.A. Nadeem, J.B. Metson, M.A. Keane, R.F. Howe1, J. Llorca, H. Idriss, Nat. Chem. 3 (2011) 489–492.

[39] O. Rosseler, M.V. Shankar1, M.K. Le Du, L. Schmidlin, N. Keller, V. Keller, J. Catal. 269 (2010) 179–190.

[40] S. Bashir, A.K. Wahab, H. Idriss, Catal. Today 240 (2015) 242–247.

[41] F. Cai, Y. Tang, H. Shen, C. Wang, A. Ren, L. Xiao, W. Gu, W. Shi, CrystEngComm 17 (2015) 1086–1091.

[42] Q. Xua, Y. Ma, J. Zhang, X. Wang, Z. Feng, C. Li, J. Catal. 278 (2011) 329–335.

[43] I. Romero Ocaña, A. Beltram, J.J. Delgado Jaen, G. Adami, T. Montini, P. Fornasiero, Inorg. Chim. Acta 431 (2015) 197–205, http://dx.doi.org/10.1016/j.ica.2015.01.033

[44] V. Gombac, L. Sordelli, T. Montini, J.J. Delgado, A. Adamski, G. Adami, M. Cargnello, S. Bernal, P. Fornasiero, J. Phys. Chem. A 114 (2010) 3916–3925.

[45] M. Jung, J. Scott, Y.H. Ng, Y. Jiang, R. Amal, Int. J. Hydrogen Energy 39 (2014) 12499–12506.

[46] P.A. Panatoyov, S.T. Burrows, J.P. Morris, J. Phys. Chem. C 116 (2012) 6623–6635.

[47] A. Matson, L. Osterlund, J. Phys. Chem. C 114 (2010) 14121–14132.

[48] C.E. Nanayakkara, J.K. Dillon, V.H. Grassian, J. Phys. Chem. C 118 (2014) 25487–25495.

[49] M.J. Muñoz-Batista, M.M. Ballari, A.E. Cassano, O.M. Alfano, A. Kubacka, M. Fernández-García, Catal. Sci. Technol. 5 (2015) 1521–1531.